

# Advanced Spotweld Failure Modelling Based on Trefftz Formulation

Thomas Heubrandtner, Gerold Rangger, Dietmar Scherjau

Vif GmbH, Technical University Graz, Graz, Austria

## Abstract:

This paper deals with an advanced model for spotwelds in finite element structures of car bodies under crash loads. The treatment is elasto-plastic, whereas the elastic part as well as the perfectly-plastic part is based on a special hybrid Trefftz element representing the entire spotweld, the cylindrical nugget, heat affected zone and an annulus made of base material. The linking to the residual finite element mesh, consisting of bilinear standard shells, is accomplished via a displacement frame, an arbitrary polygon. By definition the Trefftz-type solution satisfies a priori all governing differential equations within the element area and fulfils inner boundary conditions. The modelling of plastic deformation accounts for geometrically nonlinear behaviour (stress stiffening) within the metal sheet annulus and permits the forming of plastic hinges along the circumference of the comparatively rigid nugget. Isotropic hardening is considered by Hollomon's power law leading to a high resolution of the stress/strain field in the vicinity of the spotweld nugget, and enables the introduction of more accurate stress/strain-based failure criteria. The developed model is mapped on an auxiliary "beam spider", whose elasto-plastic parameters are adapted so that it yields nearly the same mechanical resultant behaviour including failure. We assess the numerical stability within the framework of explicit time integration using the central difference scheme.

## Keywords:

Spotweld Modelling, Spotweld Failure, Trefftz Formulation

## 1 Introduction

Today's cost pressure forces carmakers more and more to shorten and diminish development-times and -cycles, which is only possible with efficient application of simulation methods in the early phases of concept and development. So engineers are always looking for simulation tools providing an optimized cost-value ratio concerning numerical calculation time against technical benefit from its output.

It is well known that in all classical disciplines regarding numerical investigation of the mechanical behaviour of sheet metal components, which are jointed via spotwelds or rivets, the quality of modelling these joints is one of the crucial factors for their performance: The application of inaccurate jointing elements causes the loss of stiffness of BIW (Body in White) up to 35 %. On the other hand, a stress deviation of 10% in the vicinity of the spotweld nugget causes a 10 times higher error for its durability forecast, etc.

## 2 Hybrid Trefftz Formulation

Finite elements based on polynomials proved an effective tool for solving partial differential equations. However, there are problems, for which good approximated solutions can only be obtained with high effort by applying standard finite elements, or it is impossible at all. These are usually problems, whose solutions or their partial derivatives can't be approximated well by polynomials used in the finite element method. That's the case for the simulation of the mechanical behaviour of a spotweld. The linear or quadratic standard shell elements are not suited for the cylinder symmetry dominating in the surrounding area of the circular spotweld nugget. The fact, that the difficulties in finding good solutions arise from these small parts of the entire structure, suggests the introduction of special finite elements, which are adapted to the local conditions via special shape functions. Suitable for this purpose proves a coupled pair of special Trefftz elements with a circular boundary  $\Gamma_1$  within the element area  $\Omega$  (Fig.1a). As per definition the shape functions satisfy the governing differential equations within  $\Omega$ , and fulfil boundary conditions on inner boundary curves  $\Gamma_1$ . The spotweld nugget is approximately rigid compared to the adjacent sheets because the martensitic nugget has a higher yield point than the ferritic sheet, and the elastic plate bending stiffness is proportional to the 3<sup>rd</sup> power of the thickness. Thus the comparatively rigid spotweld nugget is represented by a rigid cylinder, which connects both inner circles of the Trefftz elements (Fig.1b). This linkage is implemented by coupling a pair of auxiliary nodes (Fig.1c). These lie in the center of  $\Gamma_1$ , and carry the spatial displacement and rotation of the spotweld nugget. In addition to the special spotweld elements, bilinear standard shells are arranged on uncritical sub-domains of the structure. The linking is accomplished via a displacement frame  $\Gamma_5$ , an arbitrary polygon, formed by the set of shared edges of all adjacent standard shells.

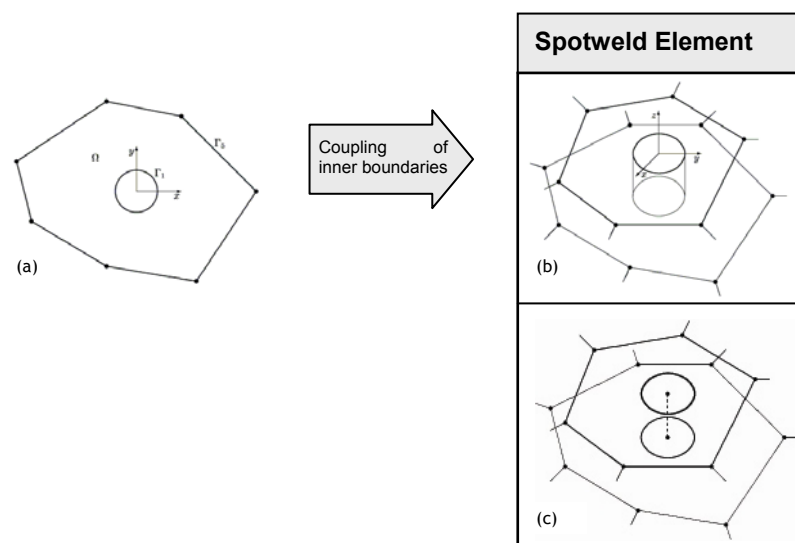


**Figure 1:** (a) The Trefftz element area  $\Omega$  with the circumference of the spotweld nugget  $\Gamma_1$ , and the polygon  $\Gamma_5$  of shared edges with all adjacent standard shells. (b) Linkage of two Trefftz elements by a rigid cylinder (spotweld nugget) is accomplished via a pair of auxiliary nodes (c).

## 2.1 Linear Elastic Deformation

It is well known, that in the case of linear elasticity the system of thin-plate equations concerning membrane- and bending-type deformations decouple completely, so they can be dealt with separately.

### 2.1.1 Membrane-type deformation

**Extension of the principle of minimal potential energy:** The essential trick is to introduce an additional term in the potential energy leading to a weak form, which transmit the essential displacement boundary condition along the polygon into natural one. Now we have two distinct displacement fields along the polygon, which are not necessarily identical. The first comes from the solutions within the element area, and the second one is the prescribed displacement field equal to the linked standard shells, for example, piece-wise linear between nodes. Minimization of the potential leads to a stiffness matrix which can be coupled with any other finite element with similar displacement assumptions.

The additional requirement of geometrical boundary conditions  $\bar{u} = \bar{\bar{u}}$  can be avoided, if the first variation of the potential is extended by an artificial term,

$$\int_{\Gamma} \delta \bar{T}^T [\bar{\bar{u}} - \bar{u}] t ds, \quad (1)$$

where  $t$  is the plate thickness and  $\bar{T}$  the traction acting along the boundary  $\Gamma$ . Both, the displacement and stress boundary conditions are now natural conditions. The weak form (1) serves as a starting point for a technique to link Trefftz elements with adjacent bi-linear standard shells (Piltner [7]). The prescribed displacement vector  $\bar{\bar{u}}$  is identified with the linear boundary displacement field  $\bar{\bar{u}}$  on the closed boundary curve  $\Gamma_5$ ,

$$\bar{\bar{u}} = \begin{pmatrix} \bar{U}^T \bar{\bar{u}} \\ \bar{V}^T \bar{\bar{v}} \end{pmatrix} = \bar{\bar{u}} \text{ on } \Gamma_5, \quad (2)$$

with nodal displacements  $\bar{\bar{u}}, \bar{\bar{v}}$ . The vectors  $\bar{U}$  and  $\bar{V}$  are defined piecewise along distinct edges of the polygon  $\Gamma_5$ , with a total of  $n$  nodes,

$$\bar{U}^T(s) = \bar{V}^T(s) = \begin{pmatrix} \left( 1 - \frac{s}{s_{1,2}}, \frac{s}{s_{1,2}}, 0, 0, \dots, 0 \right) \\ \left( 0, 1 - \frac{s}{s_{1,2}}, \frac{s}{s_{1,2}}, 0, \dots, 0 \right) \\ \vdots \\ \left( \frac{s}{s_{n,1}}, 0, 0, 0, \dots, 1 - \frac{s}{s_{n,1}} \right) \end{pmatrix}. \quad (3)$$

The first vector refers to the edge between node 1 and 2, the second between 2 and 3, etc. Lengths of edges from node  $i$  to node  $j$  are denoted by  $s_{i,j}$ , and  $s$  means the distance of an arbitrary point on an edge to its "first" corner.

### 2.1.2 Bending-type deformation

Bending is considered within the framework of Kirchhoff's theory of thin plates. Analogous extension of First variation of the potential by additional terms

$$\int_{\Gamma} \delta Q [w - \bar{w}] ds + \int_{\Gamma} \delta \bar{M}^T [\nabla w - \nabla \bar{w}] ds, \quad (4)$$

with  $Q$  and  $\bar{M}$  as force acting normal to the plate and moment twisting the boundary  $\Gamma$ , respectively (Heubrandtner et al. [2]). The prescribed bending-type displacement vector, analogous  $\bar{\bar{u}}$ , consists of the out-of-plane displacement,  $\bar{w}$ , and additional rotational degrees of freedom,  $\nabla \bar{w}$ , with respect to axes lying within the plate-plane.

### 2.1.3 Analytic solutions

Both, membrane- and bending-type deformation can be reduced to bi-harmonic functions, Airy's stress function,  $\nabla^4 U = 0$ , and out-of-plane displacement,  $\nabla^4 w = 0$ , respectively. The general solutions are presentable by the real part  $\Re[z\Phi(z) + \Psi(z)]$  with complex potentials  $\Phi$  and  $\Psi$  introduced by Kolosov-Muskhelishvili [4, 5, 1], and  $z = x + iy$ ,  $\bar{z} = x - iy$ . An analytically deduced stress field within the Trefftz element area for an exemplary load case can be seen in Fig.2.

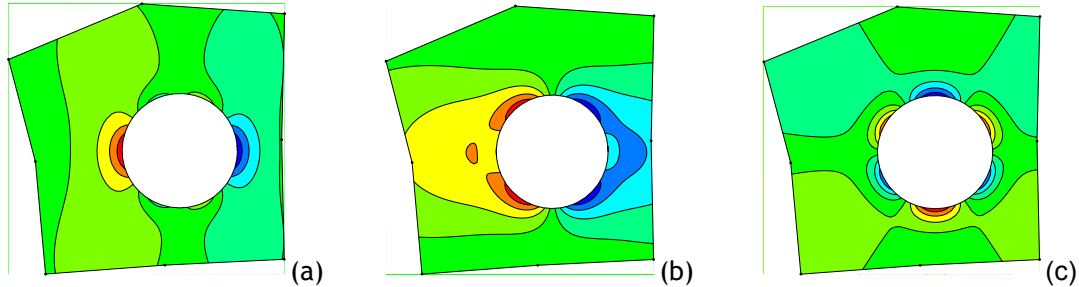


**Figure 2:** Example of contour diagrams of the stress components  $\sigma_{xx}$  (a),  $\sigma_{yy}$  (b) and  $\tau_{xy}$  (c) within the Trefftz-element area.

## 2.2 Plastic Deformation

We consider a elasto-plastic isotropic material subjected to von Mises yield surface  $\sigma'_{ij}\sigma'_{ij} = \frac{2}{3}Y^2$ , with the deviatoric stress  $\sigma'_{ij}$  and tensile yield stress  $Y$ . It is additionally assumed, that during crash load the principal stress and strain ratios are held approximately constant (Hencky conditions) in the surrounding of the spotweld nugget, so the normality principle simplifies to a non-incremental form (Hill [3])  $\varepsilon' = 3\bar{\varepsilon}/2\bar{\sigma}\sigma'$ , with deviatoric strain  $\varepsilon'$ , and equivalent strain  $\bar{\varepsilon}$  and stress  $\bar{\sigma}$ . Within the framework of Hencky plasticity the displacement field fulfils a variation principle:  $\bar{u}$  minimizes the energy functional (Anzellotti and Giaquinta [6]). For rigid-perfectly plastic materials this functional can be given in the following form,

$$E(\bar{u}) = \int_{\Omega} |\varepsilon'(\bar{u})| dV, \quad (5)$$

where  $\bar{u}$  fulfils incompressibility,  $\nabla \cdot \bar{u} = 0$ , and satisfies all boundary conditions along  $\Gamma$ . The corresponding Euler equation is simply the Laplace equation,

$$\nabla^2 w = 0, \quad (6)$$

so  $w(x, y)$  is a harmonic function within  $\Omega$ .

### 2.2.1 Thin plate kinematics in consideration of large deflection (stress stiffening)

Kinematical assumptions within the framework of thin plate approximation are reflected in the displacement field

$$\begin{pmatrix} u \\ v \\ w \end{pmatrix} = \begin{pmatrix} u_0(x, y) \\ v_0(x, y) \\ w_0(x, y) \end{pmatrix} - z \begin{pmatrix} \phi_x \\ \phi_y \\ 0 \end{pmatrix}, \quad \text{with } \frac{\partial w}{\partial x} = \phi_x, \quad \frac{\partial w}{\partial y} = \phi_y. \quad (7)$$

The Green-Lagrange strain tensor for thin plates is (Zienkiewicz and Taylor [10])

$$E = \begin{pmatrix} \frac{\partial u}{\partial x} + \frac{1}{2} \left( \frac{\partial w}{\partial x} \right)^2 & \frac{1}{2} \left( \frac{\partial u}{\partial y} + \frac{\partial v}{\partial x} + \frac{\partial w}{\partial x} \frac{\partial w}{\partial y} \right) & 0 \\ \frac{1}{2} \left( \frac{\partial u}{\partial y} + \frac{\partial v}{\partial x} + \frac{\partial w}{\partial x} \frac{\partial w}{\partial y} \right) & \frac{\partial v}{\partial y} + \frac{1}{2} \left( \frac{\partial w}{\partial y} \right)^2 & 0 \\ 0 & 0 & \frac{1}{2} \left( \left( \frac{\partial w}{\partial x} \right)^2 + \left( \frac{\partial w}{\partial y} \right)^2 \right) \end{pmatrix} - z \begin{pmatrix} \frac{\partial^2 w}{\partial x^2} & \frac{\partial^2 w}{\partial x \partial y} & 0 \\ \frac{\partial^2 w}{\partial x \partial y} & \frac{\partial^2 w}{\partial y^2} & 0 \\ 0 & 0 & 0 \end{pmatrix}, \quad (8)$$

where the strain component causing sheet thinning is determined from volume constancy. For further proceeding the area  $\Omega$  can be divided into two parts with qualitatively different predominating deformation types.

- **1 Plastic bending, plastic hinge:**

The rigid circumference of the spotweld nugget acts like a plastic hinge, so the second term in (8), the curvature, is dominant, and the corresponding plastic work becomes (for the case of no work-hardening)

$$W_p^1 \approx \frac{Yt^2}{2\sqrt{3}} \sqrt{1 + R_1^2} \oint_{\Gamma_1} \left| \frac{\partial w}{\partial n} \right| ds, \quad (9)$$

where  $\frac{\partial}{\partial n}$  means outward normal derivation along the inner circle.

- **2 Plastic stretching:**

In the course of out-of-plane deformation the first term in (8), representing the plastic membrane type deformation, becomes more and more crucial. Additional neglect of in-plane displacements yield the following expression for plastic work (for the case of no work-hardening)

$$W_p^2 = \frac{Yt}{\sqrt{3}} \oint_{\Gamma} \frac{\partial w}{\partial n} w ds \quad (10)$$

The linearity of governing differential equation (6) offers the development of a finite spotweld element by Trefftz formulation. It covers Hencky plasticity for the case of monotonic loading (Fig.3).

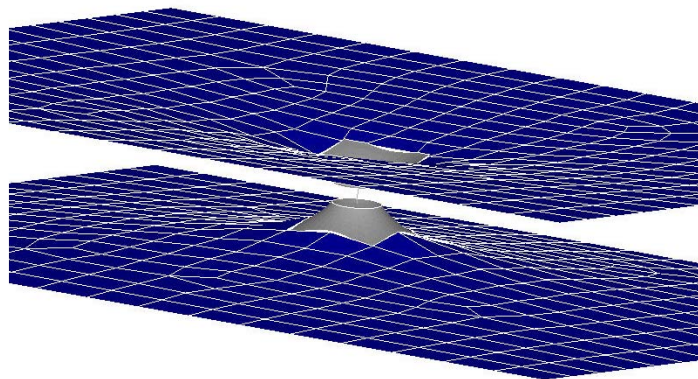


**Figure 3:** Hybrid Trefftz finite spotweld element covering Hencky plasticity. The material is rigid/perfectly plastic.

### 3 Failure (Instability) Criteria

Real tests show, that spotwelds under crash loads fail predominantly at the circumference of the nugget (within the base material) (see Fig.4). The ideal rigidity of the nugget enforces the state of plane strain on its circumference. Swift's instability law,

$$\varepsilon_{major} = n, \quad (11)$$

for the onset of local necking is used to predict spotweld failure, where  $\varepsilon_{major}$  is the major principal strain (in-plane) and  $n$  is the hardening exponent of the base material. Alternatively, the plane strain-point on the forming limit curve (FLC) of the base material can be used. The results are compared with real quasi-static tensile tests (see Table 1) and show a good coincidence between theory and experiment.

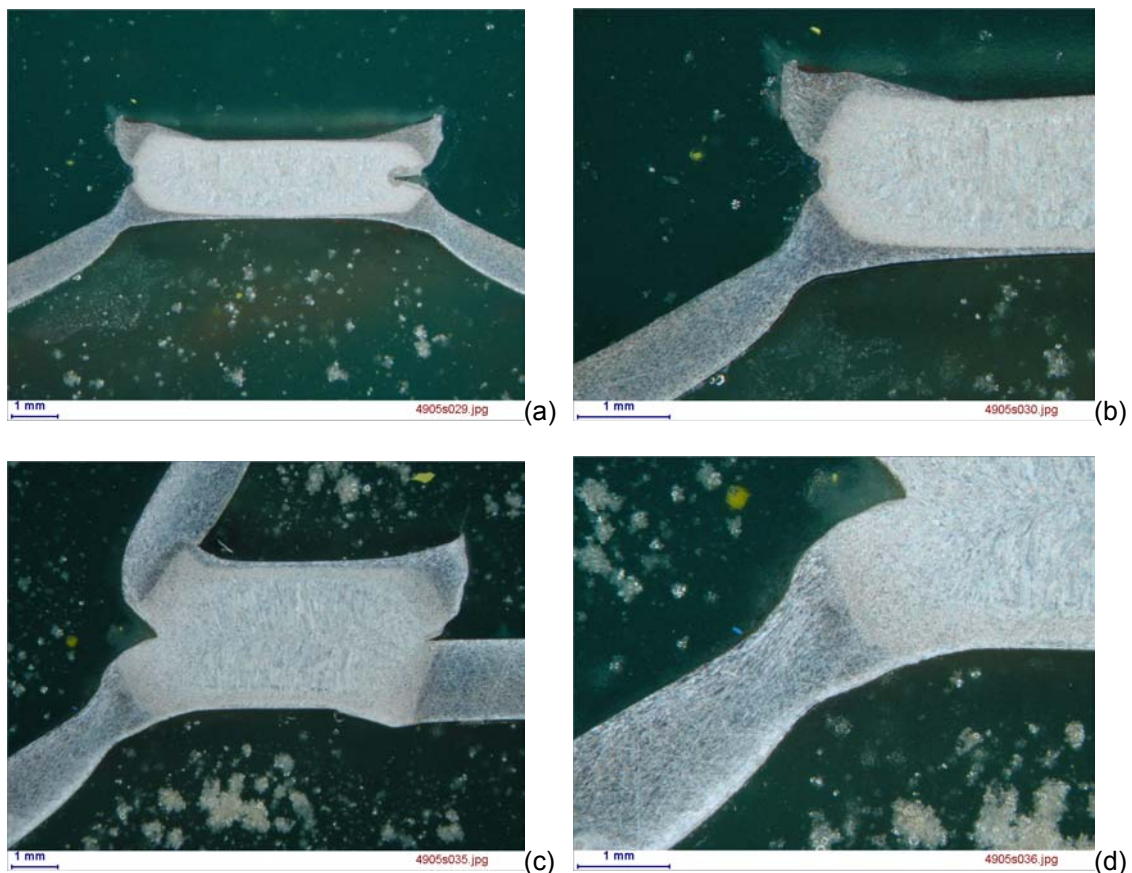


**Figure 4:** Micrographs of failed spotwelds: (a), (b) normal tension (90°-direction); (c), (b) loaded under 30°-direction. The reason for failure is the onset of local necking of the base material in the vicinity of the nugget.

#### 3.1 Three Elementary Load Cases

Three elementary load cases are investigated analytically (Heubrandtner et al. [11]):

**i) Normal Tension:** In the course of proceeding out of plane deformation the first term in (8), representing the plastic membrane-type deformation, becomes more and more crucial. Additional neglect of in-plane displacements yield the following expression for the plastic work, using Hollomon's power law for work-hardening,  $\bar{\sigma} = K\bar{\varepsilon}^n$ ,

$$W_p^2 = 3 \frac{n+1}{2} \frac{2\pi Kt}{n+1} \int_r w'(r)^{2(n+1)} r dr. \quad (12)$$

Minimization of the displacement field, assuming the conditions of Hencky plasticity are met; leads to analytical expressions for ultimate normal forces concerning stretching and bending along the spotweld nugget circumference acting as plastic hinge, respectively,

$$F_{\max}^1 = 2^{n+1} 3^{-\frac{n+1}{2}} n^{n+1} \sqrt{1 + R_1^2} \frac{\pi K t^2}{2n + 1} \left[ \left( \frac{R_2}{R_1} \right)^{\frac{2n}{2n+1}} - 1 \right]^{-1}, \quad (13)$$

$$F_{\max}^2 = 2^{n+\frac{5}{2}} 3^{-\frac{n+1}{2}} n^{n+\frac{1}{2}} \pi K R_1 t. \quad (14)$$

ii) **Shearing:** The plastic work is

$$W_p^2 = 3^{-\frac{n+1}{2}} \frac{Kt}{n+1} \int_r u'(r)^{n+1} r dr \int_0^{2\pi} (4 \cos^2 \varphi + \sin^2 \varphi)^{\frac{n+1}{2}} d\varphi, \quad (15)$$

and the corresponding ultimate force deduced from the variational principle of Hencky plasticity becomes

$$F_{\max}^2 = 3^{-\frac{n+1}{2}} n^n K t R_1 \int_0^{2\pi} (4 \cos^2 \varphi + \sin^2 \varphi)^{\frac{n+1}{2}} d\varphi. \quad (16)$$

iii) **Torsion:** In the case of torsion there arises no plain strain but a pure shear condition. So there is no plate thinning and consequently no local necking. The used failure criteria is the shear strength, approximately a half the tensile strength  $S$ . Ultimate resultant moment is deduced from the plastic work,

$$W_p^2 = 2\pi 3^{-\frac{n+1}{2}} \frac{Kt}{n+1} \int_r \left( \frac{\partial \bar{u}}{\partial r} - \frac{\bar{u}}{r} \right)^{n+1} r dr, \quad (17)$$

leading to

$$M_{\max}^2 = \pi R_1^2 t S, \quad (18)$$

which could also be obtained more directly by considering the local circumferential stress field. Comparison of measured maximum forces and corresponding analytical expressions shows a good accordance (see Fig.5, Table.1).

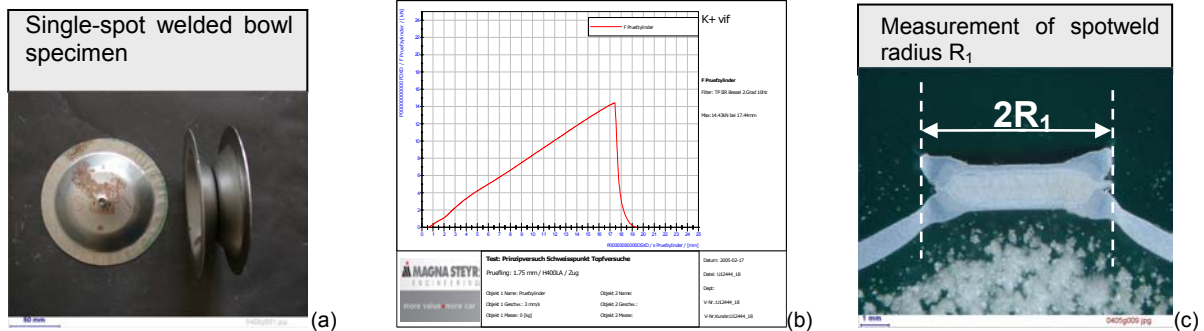


**Figure 5:** Real tensile tests with single-spot welded bowl specimen (a). Force vs. displacement is measured until total separation of the two bowls (b). The spotweld radius  $R_1$  needed for the analytical expressions for the maximum forces at failure is obtained from micrographs of the spotweld (c).

Tension				Shear			
Test#	Material	Thickness [mm]	max. Force [kN]	Test#	Material	Thickness [mm]	max. Force [kN]
1	DC04	1.00	5.47	1	DC04	1.00	7.70
2	DC04	1.00	5.29	2	DC04	1.00	7.62
3	DC04	1.00	5.46	3	DC04	1.00	7.07
Analytical	DC04	1.00	5.33	Analytical	DC04	1.00	7.50
1	H400LA	1.00	5.10	1	H400LA	1.00	8.78
2	H400LA	1.00	4.82	2	H400LA	1.00	9.47
3	H400LA	1.00	4.67	3	H400LA	1.00	10.77
Analytical	H400LA	1.00	4.85	Analytical	H400LA	1.00	9.31
1	DC04	1.75	10.52	1	DC04	1.75	13.09
2	DC04	1.75	10.70	2	DC04	1.75	13.14
3	DC04	1.75	10.95	3	DC04	1.75	13.32
Analytical	DC04	1.75	10.77	Analytical	DC04	1.75	13.12
1	H400LA	1.75	12.03				
2	H400LA	1.75	14.82				
3	H400LA	1.75	14.43				
Analytical	H400LA	1.75	14.41				

**Table 1:** Comparison of calculated and measured maximal forces at instability/failure.

### 3.2 Hybrid Load Case

To predict the failure for a general load case, which is a combination of the three basic load cases, we make the assumption, that the maximal failure values for hybrid load cases span a closed surface within the space of the three basic load cases. This can be for example an ellipsoid. The maximum quantities are obtained from (14, 16, 18).

$$\left(\frac{F^{shear}}{F_{max}^{shear}}\right)^2 + \left(\frac{M^{torsion}}{M_{max}^{torsion}}\right)^2 + \left(\frac{F^{tension}}{F_{max}^{tension}}\right)^2 \leq 1 \quad (19)$$

## 4 Implementation into LS-Dyna (Explicit Time Integration)

To make the benefit from Trefftz formulation applicable for LS-Dyna an analogous model, made of beam elements, is constructed. The elasto-plastic beam parameters are calculated automatically in such a way, that the entire structure behaves similar to the corresponding elastic-plastic Trefftz element (Fig.6). This approach has essential advantages compared to standard methods. It provides realistic kinematical behaviour of the spotweld under crash loads, for example realistic twisting of the nugget due to shear loading, because it takes its circular shape and size into account. Realistic kinematics is required to determine the position inside or outside of the failure envelope (19), and thus very important for the failure prediction. Numerical stability within the framework of explicit time integration is guaranteed by adapting the beam stiffness slightly if necessary. Analytically evaluated failure envelope (19) is used as failure criteria of the beam connecting the both mid-nodes (Fig.7)

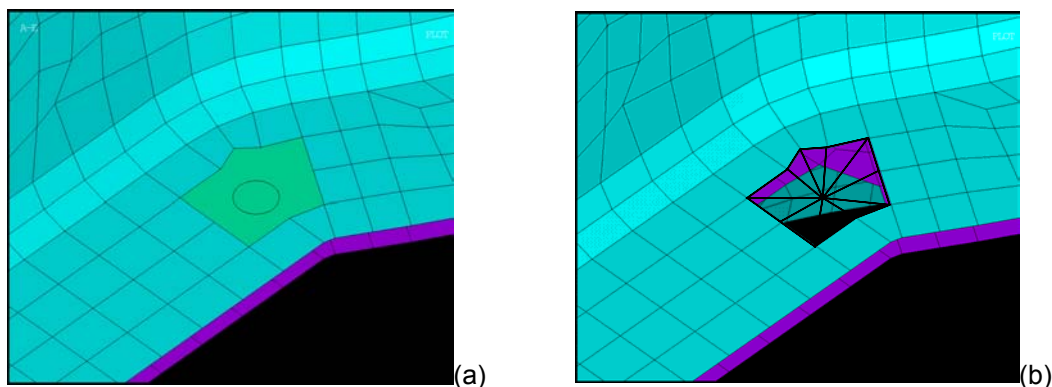


**Figure 6:** The elasto-plastic spotweld element (hybrid Trefftz finite Element) (a) is replaced by a system of beam elements, that exhibits similar resultant behaviour.

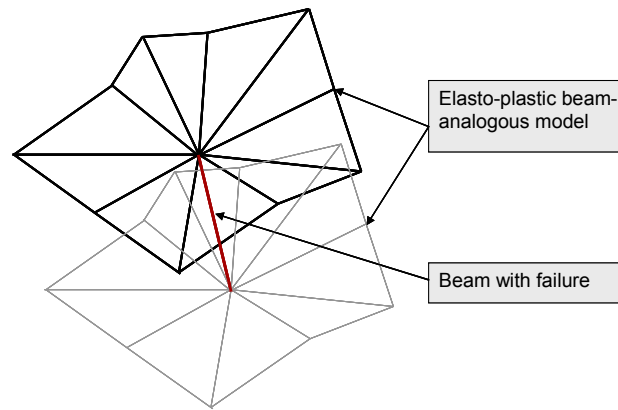


**Figure 7:** The analogous models made of beam elements are connected by a beam element including failure.

#### 4.1 Pre-Processor Tool

A pre-processor tool is developed which provides automatically setting of the spotweld elements into the independently meshed finite shell-element structure of the car body. The input data are the LS-Dyna key-file, the connectors-file, containing the information about positions and shapes of all spotwelds, and an additional file, which assigns the range of free values for all needed spotweld identification numbers. Additionally you can choose between a spotweld element, optimal for pure elasticity or plasticity including failure.

## 5 Summary

A finite spotweld element based on hybrid Trefftz formulation is developed with a rigid cylinder, representing the comparatively rigid nugget, and the surrounding area of the metal sheet, which is linked to the adjacent shell element structure via an arbitrary polygon. It covers linear elastic membrane- and bending- type deformations within the framework of Kirchhoff's thin-plate approximation. Hencky's deformation theory for a rigid-perfectly plastic material yield linear governing differential equations for the displacement field, by taking geometrical non-linear (stress stiffening) into account. Plastic bending, which is concentrated at the rigid circumference of the spotweld nugget, is incorporated into the model by means of a circular plastic hinge. The elasto-plastic properties are mapped onto an analogous structure made of standard beam elements to become applicable in Ls-dyna. Numerical stability concerning explicit time integration is guaranteed by adapting the beam stiffness slightly, if necessary. Spotweld failure (instability) due to the onset of local necking in the vicinity of the nugget is predicted analytically by Swift's law, or forming limit curves, for three elementary load cases: shear, tension and torsion. Their ultimate forces and moment span a closed failure envelope within the space of the three basic load cases. Trefftz formulation provides the advantage over standard spotweld models to offer more realistic kinematical behaviour of the spotweld nugget within the entire structure during crash loading. Its kinematical state determines the current position in the space of the three elementary load cases, whether it is inside or outside of the failure envelope.

## 6 Acknowledgement

Die Autoren danken dem K plus Kompetenzzentren-Programm vom Bundesministerium für Verkehr, Innovation und Technologie (BMVIT), Österreichische Forschungsförderungsgesellschaft mbH (FFG), Das Land Steiermark, Stadt Graz, und die steirische Wirtschaftsförderungsgesellschaft mbH (SFG) für die finanzielle Unterstützung.

Weiters bedanken wir uns bei unseren Projektpartnern MAGNA STEYR Fahrzeugtechnik AG & CO KG und der TU Graz (Institut für Werkstoffkunde, Schweißtechnik und spanloser Formgebung) für ihre Unterstützung.

## 7 References

- [1] England, AH.: "Complex Variable Methods in Elasticity", Wiley-Interscience, New York, 1971
- [2] Heubrandtner, T and Akgün T.: "Trefftz Finite Element Formulation of a Spot Weld in Dynamic Crash Calculations", 7<sup>th</sup> International Seminar Numerical Analysis of Weldability 2003, Graz-Seggau, 2003
- [3] Hill, R.: "The Mathematical Theory of Plasticity", Oxford, 1950
- [4] Kolosov, GV.: "On an Application of Complex Function Theory to a Plane Problem of the Mathematical Theory of Elasticity", Yuriev, 1909
- [5] Muskhelishvili, NI.: "Some Basic Problems of the Mathematical Theory of Elasticity", Groningen, Noordhoof, 1953
- [6] Anzellotti, G and Giaquinta, M: "On the Existence of the Fields of Stresses and Displacements for an Elasto-Perfectly Plastic Body in Static Equilibrium", J. Math. pures et appl., 61, 1982, p. 219-244
- [7] Piltner, R.: "Special Finite Elements with Holes and Internal Cracks", Int. J. for Num. Methods in Engineering 1985, 21,1471-1485
- [8] Piltner, R.: "Recent Developments in the Trefftz Method for Finite Element and Boundary Element Applications", Advances in Engineering Software 1995, 24, 107-115
- [9] Trefftz, E.: „Ein Gegenstück zum Ritz’schen Verfahren“, Proc. 2<sup>nd</sup> Int. Cong. on Applied Mechanics, Zürich 1929, 131-137
- [10] Zienkiewicz, OC. and Taylor, RL.: "The Finite Element Method - Solid Mechanics", 2<sup>nd</sup> edn., Oxford, 2000
- [11] Heubrandtner, T., Scherjau, D. and Lind, C.: "Advanced Spotweld Failure Modelling Based on Trefftz Formulation", 5<sup>th</sup> International Conference on Computation of Shell and Spatial Structures (IASS IACM 2005) Salzburg, 2005